

Loss of silent-chromatin looping and impaired imprinting of *DLX5* in Rett syndrome

Shin-ichi Horike^{1,3}, Shutao Cai^{1,3}, Masaru Miyano^{1,3}, Jan-Fang Cheng¹ & Terumi Kohwi-Shigematsu¹

Mutations in *MECP2* are associated with Rett syndrome, an X-linked neurodevelopmental disorder. To identify genes targeted by *Mecp2*, we sequenced 100 *in vivo* *Mecp2*-binding sites in mouse brain. Several sequences mapped to an imprinted gene cluster on chromosome 6, including *Dlx5* and *Dlx6*, whose transcription was roughly two times greater in brains of *Mecp2*-null mice compared with those of wild-type mice. The maternally expressed gene *DLX5* showed a loss of imprinting in lymphoblastoid cells from individuals with Rett syndrome. Because *Dlx5* regulates production of enzymes that synthesize γ -aminobutyric acid (GABA), loss of imprinting of *Dlx5* may alter GABAergic neuron activity in individuals with Rett syndrome. In mouse brain, *Dlx5* imprinting was relaxed, yet *Mecp2*-mediated silent-chromatin structure existed at the *Dlx5-Dlx6* locus in brains of wild-type, but not *Mecp2*-null, mice. *Mecp2* targeted histone deacetylase 1 to a sharply defined, ~1-kb region at the *Dlx5-Dlx6* locus and promoted repressive histone methylation at Lys9 at this site. Chromatin immunoprecipitation-combined loop assays showed that *Mecp2* mediated the silent chromatin-derived 11-kb chromatin loop at the *Dlx5-Dlx6* locus. This loop was absent in chromatin of brains of *Mecp2*-null mice, and *Dlx5-Dlx6* interacted with far distant sequences, forming distinct active chromatin-associated loops. These results show that formation of a silent-chromatin loop is a new mechanism underlying gene regulation by *Mecp2*.

Epigenetic modifications such as DNA methylation and histone modification are required for genome reprogramming during development, tissue-specific gene expression and global gene silencing. DNA methylation is essential for embryonic development in the mouse and has a role in genomic imprinting¹. Methyl-CpG binding protein 2 (*Mecp2*) is thought to selectively bind methyl-CpG dinucleotides in the mammalian genome² and to function as a transcriptional repressor *in vivo* by interacting with Sin3A and recruiting histone deacetylase (Hdac)^{3,4}. *Mecp2* associates with histone H3 Lys9 methyltransferase⁵ and with the DNA methyltransferase Dnmt1 (ref. 6), linking DNA methylation to histone methylation. Mutations in the gene *MECP2* have been identified in most individuals with Rett syndrome (RTT; OMIM 312750)^{7,8}. RTT occurs almost exclusively in females who carry heterozygous mutations in *MECP2*. The clinical features of RTT, which include hand wringing, autism, seizures and loss of speech, appear 6–18 months after birth^{9,10}. Although *Mecp2* is ubiquitously expressed, the phenotypes indicate that *Mecp2* has a crucial function in the postnatal nervous system. In support of this possibility, *Mecp2* is highly expressed in brain and its expression correlates with the maturation of neurons¹¹.

Conditional knockout of *Mecp2* in the mouse brain and in post-mitotic neurons, as well as germline loss of *Mecp2*, results in phenotypes that are similar to that of RTT^{12,13}. Furthermore, mice that carry clinically relevant mutations in the C terminus of *Mecp2* develop progressive neurological phenotypes similar to those of RTT

but milder than those of *Mecp2*-null mice¹⁴. These findings indicate that mutations in *Mecp2* might cause RTT-like phenotypes by disrupting the function of mature neurons in postnatal brain.

Promoters of many transcriptionally silent genes are methylated. *Mecp2*, which binds preferentially to methylated DNA, is predicted to be a global gene repressor on the basis of a large amount of biochemical evidence⁸. Microarray studies, however, did not identify any substantial changes in transcription levels in *Mecp2*-null mouse brains¹⁵ or clonal cell cultures from individuals with RTT¹⁶. Parental allele-specific methylation, or imprinting, is another regulatory component of gene expression. We therefore investigated whether *Mecp2* was involved in repressing transcription at only one allele of an imprinted gene. If this was the case, disruption of *Mecp2* would result in only a modest increase (by a factor of ~2) in expression of the affected imprinted genes.

Aberrations in expression of imprinted genes are involved in a number of human diseases, including Prader-Willi syndrome, Angelman syndrome characterized by neurological defects and Beckwith-Wiedemann syndrome¹⁷. There is *in vivo* evidence that *Mecp2* binds to an imprinting control region that is differentially methylated between the two alleles and is located upstream of the imprinted gene *H19* (ref. 18). Nevertheless, all imprinted genes tested to date, including *H19*, *IGF2*, *SNRPN*, *IPW* and *NDN*, maintain their normal imprinted status in the brains and T cells of individuals with RTT¹⁹.

¹Life Sciences Division, Lawrence Berkeley National Laboratory, 1 Cyclotron Road, Mail Stop 84-171, University of California, Berkeley, California 94720, USA.

²Present address: The Hospital for Sick Children, Toronto, Ontario, Canada. ³These authors contributed equally to this work. Correspondence should be addressed to T.K.-S. (terumiks@lbl.gov).

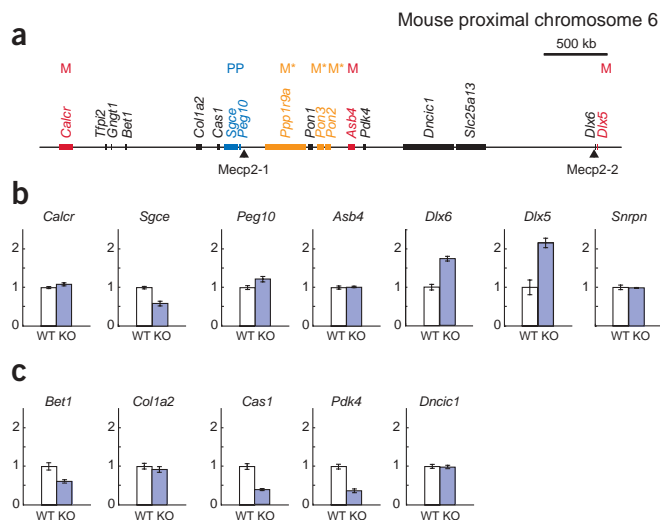


Figure 1 Ablation of *Mecp2* results in elevated transcription of *Dlx5* and *Dlx6* in the imprinted gene cluster of chromosome 6 containing *in vivo* MBSs. **(a)** Physical map of the *Calcr*–*Dlx5* imprinted gene cluster in mouse proximal chromosome 6. Previously identified genes (boxes) are positioned approximately to scale on the map. Imprinted genes are indicated by color: maternal expression, red; embryonic-specific maternal expression, orange; paternal expression, blue. P, paternally expressed genes; M, maternally expressed genes; M*, maternally expressed genes at the embryonic stages. MBSs, which were identified by urea-ChIP assay, are indicated by arrowheads. **(b)** Relative expression levels determined by quantitative RT-PCR for *Calcr*, *Sgce*, *Peg10*, *Asb4*, *Dlx6*, *Dlx5* and *Snrpn* in wild-type (WT) and *Mecp2*-null (KO) male mice (8 weeks old). *Snrpn*, located on mouse chromosome central 7, was used as a negative control, as it is unaltered in RTT cells¹⁹. Expression of *Dlx5* and *Dlx6* was higher, and expression of *Sgce* was slightly lower, in *Mecp2*-null mice than in wild-type mice. **(c)** Relative expression levels determined as in **b** for nonimprinted genes that are transcribed in the frontal cortex of wild-type (WT) and *Mecp2*-null (KO) mice. Relative expression ratios were normalized to the housekeeping gene β -actin. All reactions were done at least three times.

We used a modified chromatin immunoprecipitation (ChIP)-based cloning strategy to search for *Mecp2* target genes in mouse brain that might be dysregulated in individuals with RTT. Our strategy was based on the assumption that *Mecp2* target genes would be located close to binding sites of *Mecp2* *in vivo*. We identified *Dlx5* as a direct target gene of *Mecp2* and found that *DLX5* had lost its maternal-specific imprinted status in lymphoblastoid cells of individuals with RTT. We also found that *Mecp2* mediated histone modification and formation of a higher-order chromatin-loop structure specifically associated with silent chromatin at the *Dlx5*–*Dlx6* locus. These results identify a new role for *Mecp2* in chromatin organization and imprinting.

RESULTS

Mecp2-binding sites in a mouse chromosome 6 imprinted cluster

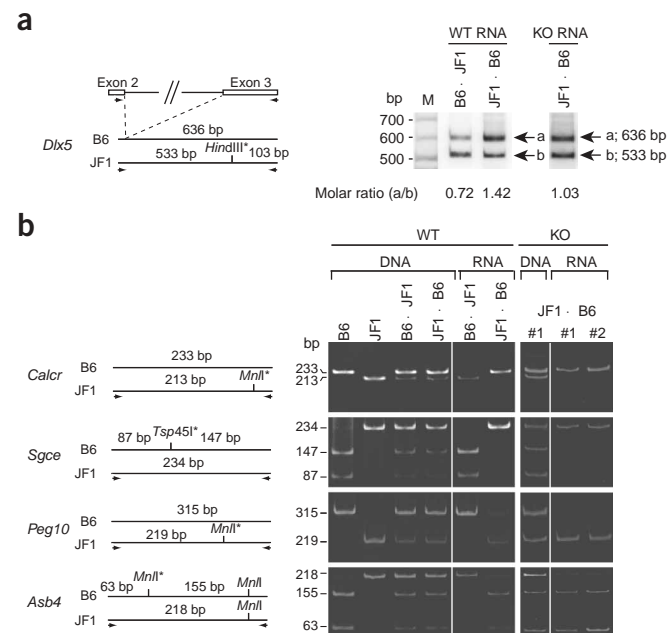
We used a ChIP method (urea-ChIP) that uses formaldehyde-crosslinked chromatin purified by urea-gradient ultracentrifugation to isolate genomic DNA sequences that bind to *Mecp2* in the brains of 1-d-old mice. This technique, which allows for identification of *in vivo* binding sequences, was previously described²⁰. We sequenced 100 *Mecp2*-binding sites (MBSs) and found multiple genes located nearby

(Supplementary Table 1 and Supplementary Note online). Of these, we cloned MBSs 10 and 11 twice each and mapped them to two sites in mouse proximal chromosome 6, which is homologous to human chromosome 7q21–22, which contains a newly identified imprinted gene cluster^{21,22}. We call MBSs 10 and 11 *Mecp2*-1 and *Mecp2*-2, respectively (Fig. 1a). This 3.5-Mbp locus contains the genes *Calcr*, *Sgce*, *Peg10*, *Ppp1r9a* (also called *Neurabin*), *Pon2*, *Pon3*, *Asb4* and *Dlx5* (refs. 21–25), which were imprinted in humans, mice or both (Fig. 1a). Whether *Dlx6* is also imprinted has not yet been determined in either humans or mice. The two MBSs are located 28 kb 3' of *Peg10* and 52 kb 3' of *Dlx5*.

Dlx5 and Dlx6 are dysregulated in cortex of Mecp2-null mice

To determine whether *Mecp2* deficiency could result in dysregulation of *Sgce*, *Peg10*, *Dlx5* or *Dlx6*, we used quantitative RT-PCR to compare their expression in the frontal cortex of wild-type and *Mecp2*-null male mice¹³. We also compared expression of the distal genes *Calcr* and

Figure 2 Preferential transcription of *Dlx5* from the maternal allele was lost in brains of *Mecp2*-null mice. **(a)** Allele-specific expression analysis for *Dlx5* using primers across exons 2 and 3. Although *Dlx5* was biallelically transcribed, there was a preference for transcription from the maternal allele in wild-type (WT) mice. This relaxed imprinting was completely lost in F₁ (JF1 × B6) *Mecp2*-null (KO) male mice. The experiment was repeated four times with reproducible results. **(b)** Allele-specific expression analyses of *Calcr*, *Sgce*, *Peg10* and *Asb4* in brains of wild-type (WT) and *Mecp2*-null (KO) male mice. Imprinting status was confirmed using F₁ hybrids from reciprocal crosses between B6 and JF1 mice (male is indicated first). Monoallelic expression of these genes was confirmed using an *MnlI* SNP for *Calcr*, *Peg10* and *Asb4* and a *Tsp45I* SNP for *Sgce*. Genomic DNA (designated DNA) and cDNA generated from RNA (designated RNA) were amplified with primers indicated by arrowheads and digested with either *MnlI* or *Tsp45I*. For *Mecp2*-null mice, one representative DNA sample and two RNA samples from two independent mice (#1 and #2) are shown. The normal parent-of-origin expression profiles were maintained for *Calcr*, *Sgce*, *Peg10* and *Asb4* in the adult brains of F₁ (JF1 male × B6 female) *Mecp2*-null male mice. All restriction fragments were analyzed by PAGE and stained with ethidium bromide, except for *Dlx5*. *HindIII*, *MnlI* and *TSP45I* sites marked with asterisks indicate SNPs.



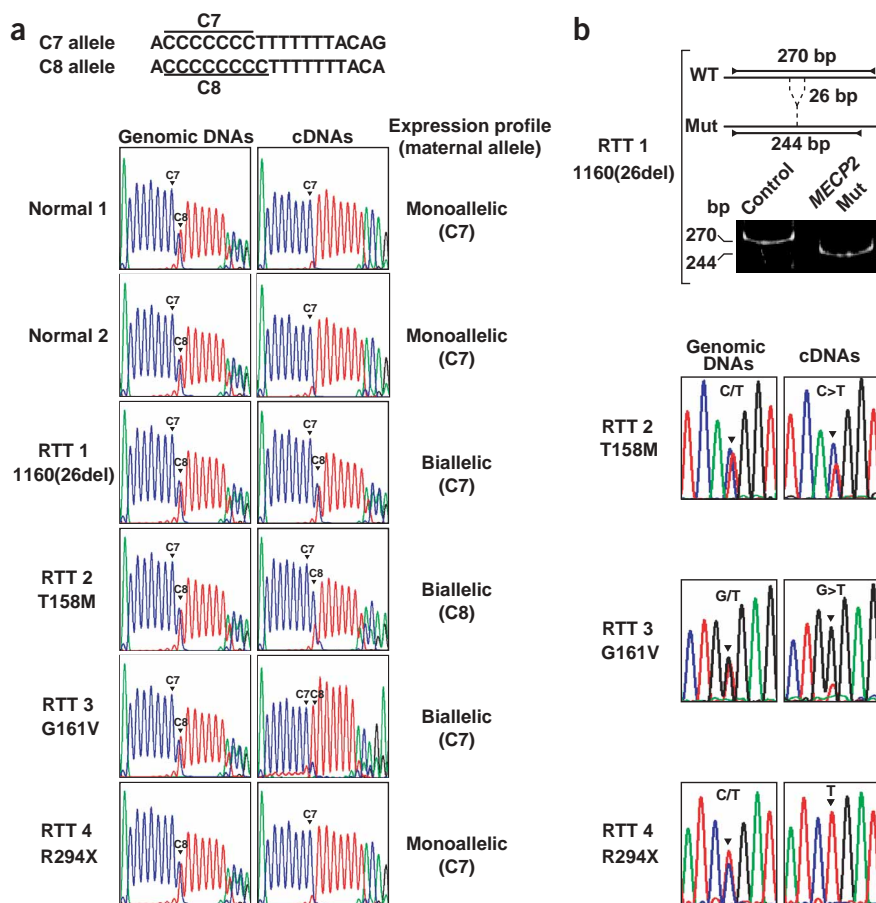


Figure 3 LOI of *DLX5* in LCLs from individuals with RTT carrying mutations in *MECP2*. (a) Allele-specific expression analysis of *DLX5*. Direct sequence analysis showed the C7 or C8 mononucleotide repeat polymorphism in the 3' UTR of *DLX5* in LCLs of four individuals with RTT. The left panels show sequence traces of genomic DNA amplified by PCR from these LCLs; the right panels show sequence traces from the RT-PCR products for *DLX5*. In normal cases, genomic DNA was heterozygous (C7 and C8 alleles) and RT-PCR products were detected from only the single parental allele (C7 allele). These results confirmed maternal allele-specific expression of *DLX5* in normal human lymphoblasts²². In individuals with RTT (RTT 1, 1160(26del); RTT 2, T158M; RTT 3, G161V), *DLX5* was biallelically transcribed from both C7 and C8 alleles. In individual RTT 4 (R294X), *DLX5* retained the normal imprinting status. (b) Expression ratios of the normal (WT) and mutated (Mut) alleles of *MECP2* in LCLs. PCR primers were designed to encompass the mutated sites in *MECP2*. The left panels show either sequence traces or fragments separated by PAGE of genomic DNA from LCLs amplified by PCR; the right panels show sequence traces from the RT-PCR products for *MECP2*. The LCL from individual RTT 1 (1160(26del)) expressed only *MECP2* transcripts from an allele carrying a 26-bp deletion. The LCLs from individuals RTT 2 (T158M) and RTT 3 (G161V) were polyclonal, expressing both normal C and mutated T alleles. The LCL from individual RTT 4 (R294X) was monoclonal, expressing only the mutated T allele.

Asb4, which are imprinted in postnatal tissues (Fig. 1b). We found no significant differences in expression of *Calcr*, *Peg10* or *Asb4* between *Mecp2*-null and wild-type mice, whereas *Sgce* was moderately downregulated in *Mecp2*-null mice. Transcription of *Dlx5* and *Dlx6* was reproducibly approximately two times higher in *Mecp2*-null mice. The *Dlx* genes belong to the *Drosophila melanogaster* Distal-less (*Dll*) homeobox gene family and are involved in various developmental processes, including limb formation and neurogenesis²⁶. Because preferential maternal expression of *Ppp1r9a*, *Pon2* and *Pon3* are restricted at embryonic stages²¹, we did not include these genes in this analysis. Analyses of nonimprinted genes at this locus showed that expression of *Col1a2* and *Dncic1* was similar in the frontal cortex of *Mecp2*-null and wild-type mice, whereas *Bet1*, *Cas1* and *Pdk4* were moderately downregulated in *Mecp2*-null mice (Fig. 1c). Downregulation of these genes in brains of *Mecp2*-null mice might be due to an indirect effect. We did not detect *Tfpi2*, *Gngt1*, *Pon1* or *Slc25a13* transcripts in mouse brains.

To examine whether *Mecp2* deficiency affected the imprinted status of *Dlx5*, potentially increasing its expression by a factor of ~2, we crossed C57BL/6J (B6) mice with JF1 mice, which carry a single-nucleotide polymorphism (SNP) in the 3' untranslated region (UTR) of *Dlx5*, and monitored parental allele-specific transcription in the F₁ offspring. There was no SNP that enabled the analysis of the potential imprinted status for *Dlx6*. The SNP found in *Dlx5* creates a *Hind*III restriction site on the JF1 allele that is absent on the B6 allele. Unlike *DLX5*, which is expressed specifically from the maternal allele in humans²², *Dlx5* in F₁ mice from crosses either of JF1 males × B6 females or of B6 males × JF1 females was biallelically transcribed in

frontal cortex (Fig. 2a) but was preferentially transcribed from the maternal allele, as determined by RT-PCR reactions followed by quantification of the PCR products (Fig. 2a). We examined whether this expression pattern persisted in brains of *Mecp2*-null mice. We crossed female B6 *Mecp2*^{+/-} mice with JF1 male mice to obtain *Mecp2*-null male F₁ mice. In these mice, *Dlx5* was equally transcribed from both parental alleles with no preference for either allele (Fig. 2a). These data indicate that ablation of *Mecp2* led to the complete loss of relaxed imprinting of *Dlx5* in mouse brain. *Mecp2* deficiency did not alter the parental allele-specific expression of the other imprinted genes (*Calcr*, *Sgce*, *Peg10* and *Asb4*) in the same gene cluster (Fig. 2b).

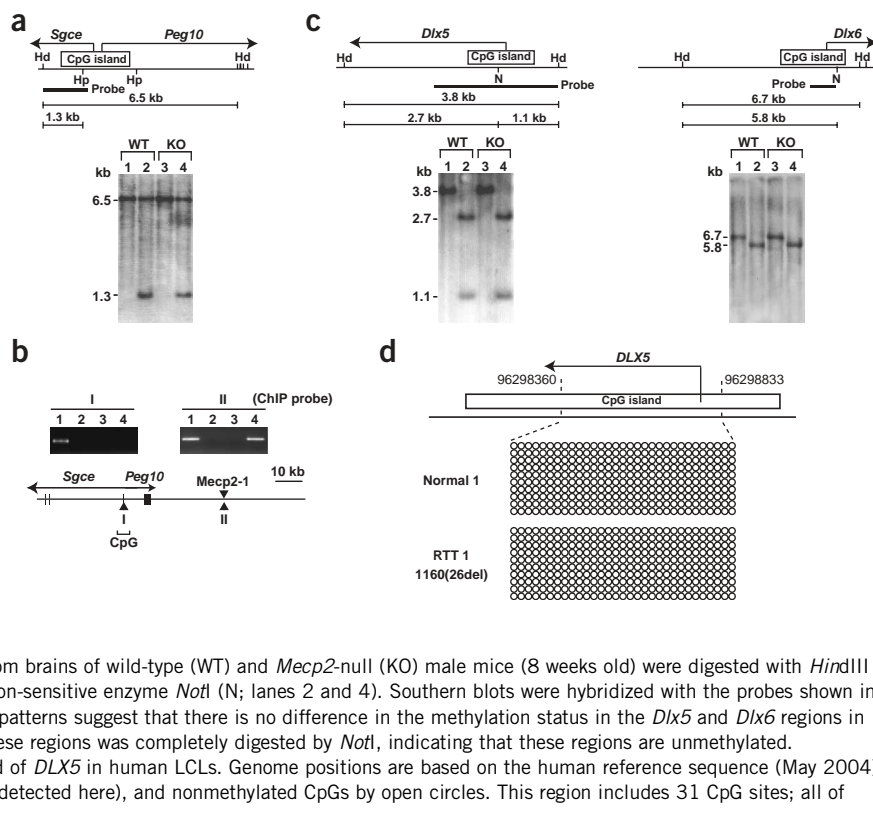
Loss of imprinting of *DLX5*

Because *DLX5* is imprinted in normal human lymphoblasts as well as in brain²², we asked whether loss of imprinting (LOI) for this gene could be found in lymphoblastoid cells from individuals with RTT who have mutations in *MECP2* and determined that it could. Using a polymorphism of either C7 or C8 repeats in the 3' UTR of *DLX5* as a marker, we screened a total of nine lymphoblastoid cell lines (LCLs) from individuals with RTT and identified four individuals who were heterozygous with respect to this polymorphism. Direct sequencing analysis of RT-PCR products from LCLs taken from these individuals showed that three of the four samples had biallelic expression of *DLX5*.

Several *de novo* missense and nonsense mutations in various regions of *MECP2* have been associated with RTT, including mutations in the methyl-DNA-binding domain (MBD), the transcriptional repressor domain and the C-terminal region^{7,10}. LCLs carrying the *MECP2* mutation 1160(del26) showed a complete LOI, expressing

Figure 4 Methylation patterns are similar in the *Dlx5-Dlx6* locus in brains of wild-type and *Mecp2*-null mice. (a) Southern-blot analysis of the 5' CpG island of *Sgce-Peg10*. Genomic DNA from brains of wild-type (WT) and *Mecp2*-null (KO) male mice (8 weeks old) were digested with *Hind*III (Hd; lanes 1 and 3) or with *Hind*III and the methylation-sensitive enzyme *Hpa*II (Hp; lanes 2 and 4). Southern blots were hybridized with the probes shown in the restriction maps.

(b) Urea-ChIP analysis for *Mecp2* binding to the *Sgce-Peg10* locus. Using formaldehyde-crosslinked frontal cortex of mouse brains, urea-ChIP was done with either nonimmune serum or antibody to *Mecp2* using primers for the CpG island sequences closely located at *Peg10* (I) and one of the original MBSs (II) near *Peg10*. PCR amplification using specific set of primers was done with genomic DNA control (lane 1), water control (lane 2), the chromatin fraction immunoprecipitated with preimmune serum (lane 3) and the chromatin fraction immunoprecipitated with antibody against *Mecp2* (lane 4). Only the cloned MBS showed positive signals for immunoprecipitated chromatin with antibody to *Mecp2*. (c) Southern-blot analysis of the 5' CpG island of *Dlx5* and *Dlx6*. Genomic DNA from brains of wild-type (WT) and *Mecp2*-null (KO) male mice (8 weeks old) were digested with *Hind*III (Hd; lanes 1 and 3) or with *Hind*III and the methylation-sensitive enzyme *Not*I (N; lanes 2 and 4). Southern blots were hybridized with the probes shown in the restriction maps. The similar restriction digestion patterns suggest that there is no difference in the methylation status in the *Dlx5* and *Dlx6* regions in brains from these two mice. Also, genomic DNA in these regions was completely digested by *Not*I, indicating that these regions are unmethylated. (d) Bisulfite analysis for methylation in the CpG island of *DLX5* in human LCLs. Genome positions are based on the human reference sequence (May 2004). Methylated CpGs are indicated by filled circles (none detected here), and nonmethylated CpGs by open circles. This region includes 31 CpG sites; all of these are unmethylated.



similar levels of *DLX5* from both alleles, whereas LCLs carrying the *MECP2* mutations T158M or G161V, which lie in the MBD, expressed lower levels of *DLX5* from the paternal allele. Another *MECP2* mutation observed in individuals with RTT (R294X), which occurs in the transcriptional repressor domain, did not affect imprinting status, as *DLX5* was transcribed almost exclusively from the maternal allele (Fig. 3a).

Because it is not known which X chromosome becomes active in a given LCL, and because LCLs obtained for this study are not necessarily monoclonal in nature, we determined whether the mutant form of *MECP2* was transcribed in each LCL sample and, if so, determined the proportion of mutant *MECP2* to wild-type *MECP2* (Fig. 3b). The R294X form of *MECP2* was exclusively transcribed in the LCLs, indicating that this mutation does not alter the imprinting of *DLX5*. LCLs that carried the 1160(del26) mutation were also monoclonal: only the mutant form of *MECP2* was expressed, leading to complete LOI. On the other hand, the two LCLs that carried mutations in the *MECP2* region encoding the MBD expressed both wild-type and mutant *MECP2*, indicating that there were two types of LCL in the samples. The proportion of wild-type *MECP2* to mutant *MECP2* (Fig. 3b) correlated well with the level of expression of *DLX5* from the paternal allele (Fig. 3a), indicating that LCLs that express either mutant form of *MECP2* underwent complete LOI. These findings show that in LCLs isolated from individuals with RTT, LOI of *DLX5* occurs as a result of some, but not all, mutations in *MECP2*. Furthermore, in all LCLs from individuals with RTT that we examined, the imprinted status of the control genes *IGF2* and *KCNQ1OT1* (also called *LIT1*) was maintained (Supplementary Fig. 1 online). LOI seems to occur specifically at *DLX5* in individuals with RTT. We also observed increased *DLX5* transcript

levels in LCLs from all four individuals with RTT (Supplementary Fig. 1 online).

The *Dlx5* and *DLX5* CpG islands are unmethylated

To understand the increased expression of *Dlx5* in brains of *Mecp2*-null mice, we first analyzed the differentially methylated region (DMR) in the CpG island associated with the first exons of *Peg10* and *Sgce*²¹. Because this DMR is established in germ cells²¹, it might be an imprinting control region, capable of regulating imprinting of distal genes. *Mecp2* associates with *Dnmt1* (ref. 6), which is important for maintenance of DNA methylation¹. Therefore, in the absence of *Mecp2*, the differentially methylated status of the DMR might be affected. Southern-blot analysis using methylation-sensitive enzymes showed that the methylation status of the DMR was unchanged in *Mecp2*-null mice (Fig. 4a). Furthermore, urea-ChIP analysis showed that the CpG island was not bound to *Mecp2* *in vivo* but was bound to the initially isolated MBS *Mecp2*-1 *in vivo* (Fig. 4b). These data suggest that *Dlx5* expression is not regulated by *Mecp2* through the DMR associated with *Peg10* and *Sgce*.

We next examined the methylation status of the CpG islands 5' to *Dlx5* and *Dlx6* in mouse brain. If their CpG islands contain methylated CpG dinucleotides, *Mecp2* may regulate *Dlx5* and *Dlx6* through binding to their CpG islands. Unexpectedly, the CpG islands were unmethylated in both alleles in brains of wild-type and *Mecp2*-null mice (Fig. 4a-c). We also examined the methylation status of the *DLX5* CpG island in LCLs by sequencing the bisulfite-modified DNA region containing the CpG island and found that this region was totally unmethylated (Fig. 4d).

Our results indicate that, whether *DLX5* is completely imprinted (as in human LCLs) or has relaxed imprinting (as in mouse brain),

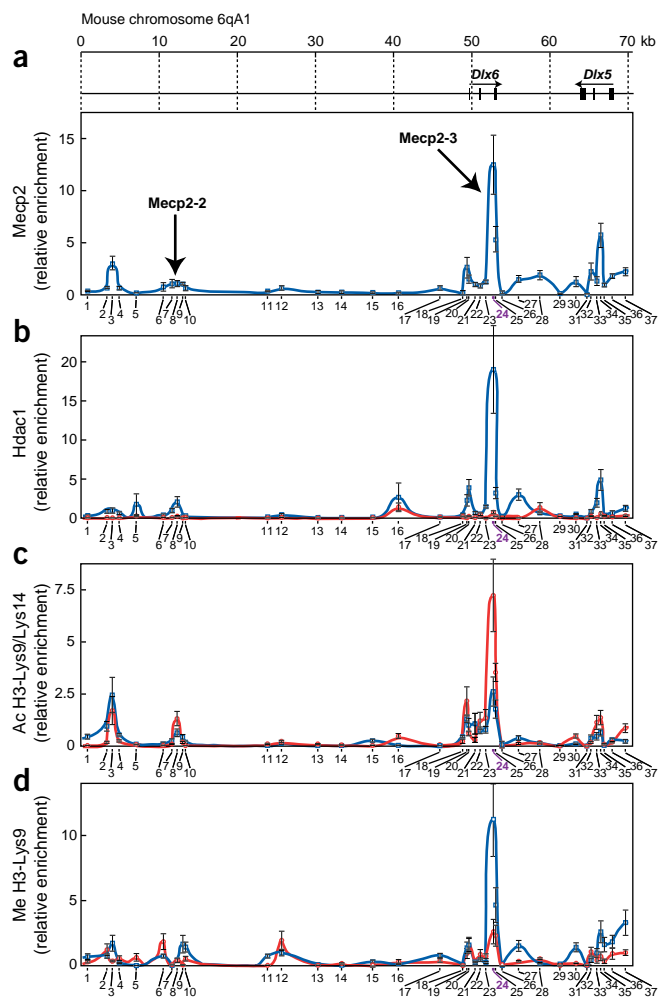


Figure 5 MeCP2 recruits Hdac1 and mediates dimethylation at H3-Lys9 at the *Dlx5-Dlx6* locus. *In vivo* chromatin structure analysis was done by urea-ChIP across the 70-kb region containing *Dlx5* and *Dlx6* of mouse chromosome 6qA1. Urea gradient-purified, formaldehyde-crosslinked chromatin from mouse brains was digested with *Sau3A*I, and the resulting chromatin fragments were immunoprecipitated using antibody against (a) MeCP2, (b) Hdac1, (c) acetylated (Ac) H3-Lys9/Lys14 and (d) dimethylated (Me) H3-Lys9. PCR amplification was done using the oligonucleotide primer sets (numbers 1–37). Blue line, wild-type mice; red line, *MeCP2*-null mice.

the corresponding CpG islands are unmethylated. Therefore, other sites must serve as a target region through which MeCP2 regulates *Dlx5* expression.

MBSs delineated by high-resolution urea-ChIP

The MeCP2-2 sequence, located 52 kb downstream of *Dlx5*, was not necessarily the only sequence near *Dlx5-Dlx6* to which MeCP2 binds. To identify all MBSs at the *Dlx5-Dlx6* locus, we carried out high-resolution urea-ChIP, analyzed by real-time PCR, throughout the 70 kb of the *Dlx5-Dlx6* interval. Using an antibody to MeCP2, this method identified a MBS in an intron of *Dlx6* (called MeCP2-3) from uniquely high PCR amplification signals at this site (Fig. 5a). This MeCP2-3 site was only 580 bp in length (distance between primers 24 and 25). Several other regions in these 70 kb of genomic DNA also had moderate to low levels of MeCP2 binding.

We searched for differentially methylated sites by sequencing bisulfite-modified DNA for selected regions that not only bound MeCP2 but were also moderately enriched in CpG dinucleotides. We verified that CpG islands associated with *Dlx5* and *Dlx6* were unmethylated (Supplementary Fig. 2 online). Regions MeCP2-2 and MeCP2-3, as well as the region of moderate MeCP2 binding in *Dlx5*, all contained methylated CpG dinucleotides, but there was no apparent difference between the two alleles in these regions (Supplementary Fig. 2 online). The sequencing data indicate that methylation status was unchanged in cortex of *MeCP2*-null mice. Furthermore, there was no difference in the methylation status between the two alleles in the brains of wild-type mice, at least in the MeCP2-bound regions and the CpG-containing regions that we examined.

We also studied the methylation status of the human sequences orthologous to the mouse MBS located in the *Dlx6* intron. We found no differential methylation between the two parental alleles in the *DLX6* intronic sequences in human LCLs (Supplementary Fig. 2 online).

MeCP2 function in region-specific histone modification

We next examined whether MeCP2 helps to establish specific chromatin structures at the *Dlx5-Dlx6* locus in mouse brains. MeCP2 associates with Hdacs^{3,4} and histone methyltransferases⁵ and is proposed to contribute in chromatin silencing, but this has not been genetically and biochemically demonstrated *in vivo*. Using a high-resolution urea-ChIP method, we examined Hdac1-binding loci to determine whether there were changes in the overall histone modification pattern at this 70-kb region when MeCP2 activity was lost. In brains of wild-type mice, the main Hdac1-binding sites (Fig. 5b) almost completely coincided with MeCP2-3 (both occurred in the intron of *Dlx6*), but in brains of *MeCP2*-null mice, Hdac1 binding was almost completely lost (Fig. 5b). These data indicate that MeCP2 recruits Hdac1 to a narrowly defined region of genomic DNA.

We determined the histone modification pattern throughout this 70-kb region of the *Dlx5-Dlx6* locus in brains of wild-type and *MeCP2*-null mice. The N-terminal tails of histones H3 and H4 are the main targets for post-translational acetylation and methylation. Acetylation of histone H3 at Lys9 (H3-Lys9) and Lys14 (H3-Lys14) is associated with transcriptionally active chromatin, whereas methylation at H3-Lys9 is an epigenetic hallmark for transcriptionally silent chromatin²⁷. Again, we used the urea-ChIP method, using antibodies against diacetylated H3-Lys9/Lys14 or against dimethylated H3-Lys9. In brains of both wild-type and *MeCP2*-null mice, acetylation of histone H3 completely coincided with MeCP2-3. Acetylation of histone H3 at this region was elevated in brains of *MeCP2*-null mice compared with those of wild-type mice (Fig. 5c). In fact, the overall level of acetylation of histone H3 was higher throughout the *Dlx5-Dlx6* locus in *MeCP2*-null mice.

Dimethylation at H3-Lys9 also occurred at MeCP2-3 in brains of wild-type mice, presumably representing transcriptionally silent chromatin (Fig. 5d), but was greatly reduced at this site, and largely reduced throughout the 70-kb region, in brains of *MeCP2*-null mice. The histone modifications (acetylation and methylation) occurred over a sharply defined area of less than 600 bp in the 70-kb region.

Our ChIP results could not be analyzed in an allele-specific manner, even at the representative MBSs, owing to the lack of a SNP (data not shown). Nevertheless, we delineated the MeCP2-3 sequence to be a narrowly defined region of Hdac1 binding and histone H3 acetylation and methylation that differed between wild-type and *MeCP2*-null mice. Taken together, these findings indicate

that *Mecp2* is required for methylation at H3-Lys9 at specific sites in a 70-kb region, particularly in the intronic region of *Dlx6*. This process probably establishes a transcriptionally silent chromatin structure. In *Mecp2*-null cells, only chromatin structure with acetylation at H3-Lys9 and H3-Lys14, resulting in increased *Dlx5* expression, could be detected.

Mecp2-null cells lack a silent chromatin-associated loop

We next explored the potential role of *Mecp2* in higher-order loop organization in the 70-kb region. If remote sequences are physically

located close together as a result of higher-order folding of chromatin *in vivo*, they may be trapped in the same restriction enzyme-digested fragments of urea-purified crosslinked chromatin. Referring to the well-defined MBSs determined by urea-ChIP, we designed multiple sets of primers to test whether any of these MBSs were brought together to form loops. If so, two such distal sequences trapped in the same chromatin fragment could be ligated and then amplified by PCR using appropriate primer sets.

We tested this using the chromosome conformation capture (3C) method^{28,29} on urea gradient-purified crosslinked chromatin²⁰. We

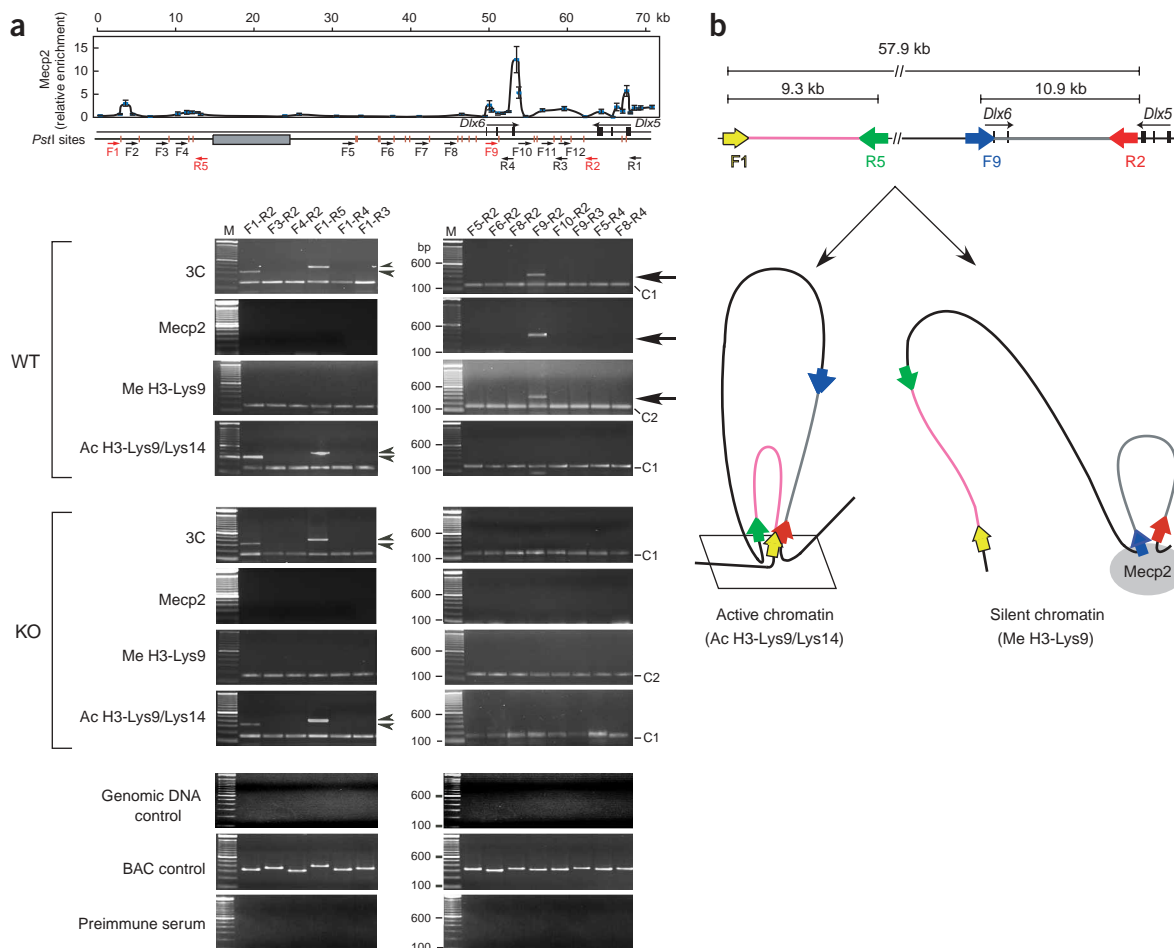


Figure 6 *Mecp2* is required for organization of the silent-chromatin loop in the *Dlx5-Dlx6* locus. (a) 3C and ChIP-loop assays were done on the 70-kb region containing the *Dlx5-Dlx6* locus. Crosslinked chromatin purified by urea ultracentrifugation was digested with *PstI* and immunoprecipitated with preimmune serum or with antibodies against *Mecp2*, against methylated (Me) H3-Lys9 or against acetylated (Ac) H3-Lys9/Lys14 (as indicated on left). The immunoprecipitated samples were diluted in a ligation buffer and ligated with T4 DNA ligase. After reversing crosslinks, the ligated DNA was amplified by PCR with various combinations of primers as indicated. 3C indicates chromatin treated as described above, except that no immunoprecipitation was done. Arrows indicate specific PCR products generated from wild-type chromatin, which were absent in *Mecp2*-null chromatin. Arrowheads indicate PCR products present in both wild-type and *Mecp2*-null chromatin. These fragments were sequenced to confirm that the two primer sequences were ligated properly. C1 and C2 indicate PCR products derived from primers from the β -actin and β -globin loci, respectively, used as internal controls for DNA loading, proper *PstI* digestion and ligation. The gray box on the top panel adjacent to R5 primer indicates ~ 10 kb of unknown sequence. Purified genomic DNA (as negative control) and cloned BAC DNA containing the 70-kb region (as positive control) after *PstI* digestion and ligation were used as templates for PCR amplification using various combination of primers shown. No PCR products could be formed from these distant sequences using purified genomic DNA, whereas all primer combinations tested could be properly amplified using the BAC clone owing to high molar concentration of fragments. (b) A model of transcription status-specific loop organization at the *Dlx5-Dlx6* locus. The ChIP-loop assay identified the *Mecp2*-associated F9-R2 interaction, with a 10.9-kb intervening chromatin loop, which was absent in *Mecp2*-null chromatin. This F9-R2 loop was also associated with chromatin enriched in dimethylated (Me) H3-Lys9, suggesting that it is derived from silent chromatin. *Mecp2*-null chromatin had distinct types of long-range interactions, such that R2 was associated with F1, which is located 57.9 kb away. The R5 sequence also participated in this three-dimensional organization, presumably forming at least a double-loop cluster. These interactions were found in wild-type chromatin as well. Because F1-R2 and F1-R5 interactions were associated with acetylated (Ac) H3-Lys9/Lys14, these interactions are probably derived from active chromatin. All experiments were repeated six to ten times, and the data shown were reproducible.

also used a new approach, applying the 3C method to the restriction enzyme-digested, urea gradient-purified crosslinked chromatin after it was immunoprecipitated with a specific antibody. This ChIP-combined chromatin-loop analysis (urea-ChIP-loop assay) presumably permits the analysis of specific chromatin pools, either transcriptionally silent chromatin associated with Hdac1 and histone methylation or active chromatin associated with histone acetylation.

We digested urea-purified crosslinked chromatin isolated from brains of wild-type mice with *Pst1* and immunoprecipitated it by antibody against *Mecp2*. We then ligated this DNA and amplified it by PCR using the combination of primers shown in **Figure 6a**. We reproducibly detected amplified signals of the expected lengths using primers F9 and R2 but did not detect signals using other primers indicated in **Figure 6a** in combination with R2 for *Mecp2*-bound chromatin fragments. Also, other reverse primers (R1, R3 and R4) never gave rise to any amplified signals using *Mecp2*-immunoprecipitated chromatin. These results show that the loop formation is mediated by highly selective sites. We sequenced the band that was amplified with primers F9 and R2 and confirmed that these two sequences corresponding to primers F9 and R2 were adjacent to each other, indicative of the formation of an 11-kb loop at the *Dlx5-Dlx6* locus. Using whole crosslinked chromatin from wild-type mice without immunoprecipitation (3C assay), we also reproducibly detected the 11-kb loop captured by F9 and R2 primers. In chromatin isolated from *Mecp2*-null cells, in contrast, we never detected the loop. Therefore, the 11-kb F9-R2 loop is probably derived from transcriptionally silent chromatin. Control studies showed that these differences between wild-type and *Mecp2*-null cells were not caused by the use of different amounts of DNA in the analysis or by incomplete digestion or ligation (**Fig. 6a**).

We next analyzed chromatin from wild-type and *Mecp2*-null cells by the urea-ChIP-loop assay after immunoprecipitation with antibodies against either acetylated H3-Lys9/Lys14 or dimethylated H3-Lys9. Using dimethylated H3-Lys9 chromatin isolated from brains of wild-type mice, we again detected the 11-kb F9-R2 loop. No other loop structure was detected with any other combination of primers. We again confirmed the sequence of the PCR product with F9 and R2 primers. In contrast, the 11-kb F9-R2 loop was not found in dimethylated H3-Lys9 chromatin immunoprecipitated from *Mecp2*-null cells.

In acetylated H3-Lys9/Lys14 chromatin isolated from brain samples from both wild-type and *Mecp2*-null mice, we obtained amplification signals of the correct sizes between F1 and R2, indicative of the formation of a 58-kb loop. We also detected this 58-kb loop in chromatin from brain tissues from both wild-type and *Mecp2*-null mice before immunoprecipitation (3C assay). In addition, using the R5 primer, we detected the presence of a smaller loop of ~9.3 kb between F1 and R5 in whole chromatin by the 3C assay in samples from both wild-type and *Mecp2*-null mice. We detected this 9.3-kb loop specifically in acetylated H3-Lys9/Lys14 chromatin but not in dimethylated H3-Lys9 chromatin immunoprecipitated from both cell types. These data indicate that for the 70-kb genomic region examined, the transcriptionally active chromatin reaches out to a distant region to form larger loop domains, whereas in silent chromatin, the loop is restricted to the immediate neighborhood of the *Dlx5-Dlx6* locus.

Our data suggest that the three-dimensional chromatin structure at the *Dlx5-Dlx6* locus consists of different loop structures, which may reflect the transcriptional status of the genes represented by the specific histone modification pattern. The transcriptionally active chromatin, marked by acetylated H3-Lys9/Lys14, contains both the large 58-kb loop (identified by primers F1-R2) and the small 9.3-kb

subloop (identified by primers F1-R5), and probably forms at least a double-loop configuration as a result of multiple remote sequences being brought into close spatial proximity. On the other hand, the silent chromatin, marked by dimethylated H3-Lys9, contains only an 11-kb loop (identified by primers F9-R2), indicating that the long-range sequence interaction is restricted to *Dlx5* and *Dlx6*. A model based on our data is shown in **Figure 6b**. Because chromatin from brain cells of *Mecp2*-null mice totally lack the specific 11-kb loop configuration associated with dimethylated H3-Lys9, *Mecp2* probably determines the higher-order folding of silent chromatin.

DISCUSSION

This study links RTT with genome imprinting by identifying a maternally expressed gene, *DLX5*, as a target for MECP2. We identified LOI for *DLX5* in three of four LCLs isolated from individuals with RTT. Using a mouse model for RTT and control mice, we analyzed *in vivo* chromatin structure across the 70-kb region that contains *Dlx5* and *Dlx6*. We found that *Mecp2* was essential for the formation of silent-chromatin structure at the *Dlx5-Dlx6* locus by specifying histone methylation at H3-Lys9 and organizing a chromatin loop specific to silent chromatin.

The identification of *DLX5* as a MECP2 target gene could provide clues to understanding mechanisms of RTT pathogenesis. In the forebrain, the *Dlx* genes are expressed by virtually all GABAergic neurons. Ectopic expression of *Dlx2* and *Dlx5* in cortical neurons induced the expression of glutamic acid decarboxylases, enzymes that synthesize GABA³⁰. In addition, *Dlx1 Dlx2* double mutant mice have reduced expression of GAD67 in the lateral ganglionic eminence (anlage of the striatum and other subcortical structures; I. Cobos and J. L. Rubenstein, unpublished observations). GABA neurotransmission has been linked to other neurodevelopmental disorders, including Angelman syndrome, which has some clinical similarity to RTT³¹.

The mouse and human *DLX* genes (*DLX1-DLX6*) are found in three convergently transcribed pairs. The largely coincident expression of the members of each pair is indicative of the existence of shared regulatory elements. Consistent with this idea, transcription of both *Dlx5* and *Dlx6* was approximately two times greater in the frontal cortex of *Mecp2*-null mice. Four of the genes (*Dlx1*, *Dlx2*, *Dlx5* and *Dlx6*) are expressed during brain development. Expression of *Dlx1* and *Dlx2* precedes that of *Dlx5* and *Dlx6*, which are expressed in the progenitors of the subventricular zone and by newly produced neurons undergoing postmitotic differentiation²⁶. A cross-regulatory cascade among different *Dlx* family members has been reported³⁰. Therefore, even a modest increase in *DLX5* expression, caused by LOI, could conceivably have a profound effect by altering expression of other *DLX* genes. This might eventually contribute to the neurological phenotypes associated with RTT. It is possible that LOI of *DLX5* could affect the GABA neurotransmission system, providing an explanation for the phenotypic similarity between RTT and Angelman syndrome. Other studies have shown that *Mecp2* regulates expression of the gene encoding brain-derived neurotrophic factor^{32,33}. Further studies are necessary to determine whether loss of MECP2 function disrupts the expression or activity of a single gene product to lead to RTT or whether this process involves a combination of events.

Notably, two chromosomal regions associated with autism on chromosomes 2q and 7q contain the *Dlx1-Dlx2* and *Dlx5-Dlx6* loci, respectively³⁴. LOI of *DLX5* might therefore also contribute to autism. In addition to complex neurological disorders, osteoporosis also occurs frequently in girls with RTT³⁵. Because the *Dlx* genes also have a role in osteogenesis²⁶, deregulated expression of *DLX5* might contribute to this aspect of RTT.

The identification of MECP2 as an enzyme that mediates imprinting of *DLX5* is important, as imprinted genes have not been found to be affected in RTT¹⁹. Our results indicate, however, that *Mecp2* is very selective, at least in the brain, and that only a small subset of imprinted genes, including *Dlx5*, is affected by the loss of *Mecp2* function. This is similar to the mouse Polycomb group protein *Eed* (embryonic ectoderm development), required for X inactivation, which also regulates a small subset of autosomal imprinted genes³⁶. In mice, *Dlx5* is transcribed from both parental alleles, consistent with a recent report³⁷, but transcription from the maternal allele is subtly favored. Nevertheless, *Dlx5* expression was approximately two times higher in brains of *Mecp2*-null mice than in those of wild-type mice. We showed that *Mecp2* targets Hdac1 to a specific site in the *Dlx5-Dlx6* locus and mediates region-specific histone methylation at H3-Lys9. In a 70-kb region of chromatin isolated from brains of *Mecp2*-null mice, Hdac1 was not associated with chromatin and histone H3 was predominantly acetylated at this site. This shows that transcriptionally silent chromatin structure exists in wild-type mice but is absent in *Mecp2*-null mice, despite the fact that *Dlx5* is biallelically transcribed in both. In contrast to human LCLs, where silent chromatin is restricted to the paternal alleles, our data suggest that in mice, both parental alleles form active chromatin as well as silent chromatin, and the loss of silent chromatin from both alleles upon *Mecp2* ablation probably accounts for the elevated *Dlx5* expression in the brains of *Mecp2*-null mice.

Although *Dlx5* is biallelically transcribed in mouse brains, if CpG methylation was required for *Mecp2* to establish silent chromatin, we expected to detect two chromatin populations that were differentially methylated, at least in MBSs. We found no evidence for such differential methylation (Fig. 4 and Supplementary Fig. 2 online). This was also true for the human sequence orthologous to the MBS in the intron of *Dlx6*. Furthermore, the CpG island of *DLX5* was unmethylated in both LCLs from individuals with RTT and from unaffected individuals, as in brains of wild-type and *Mecp2*-null mice. Similar to our observations, imprinting in the placenta has been reported to involve repressive histone methylation independent of DNA methylation³⁸. There might be mechanisms, not necessarily mediated by CpG methylation, but at the level of noncoding antisense RNAs and higher-order chromatin structure, that regulate individual genes in a large imprinted cluster. We found that Hdac1 recruitment and histone modification at the *Dlx5-Dlx6* locus in brains of wild-type mice were confined to a narrow region of <1 kb that coincided with the MBS. In the 70-kb region that we examined, *Mecp2* specifically marked a region <1 kb in the *Dlx5-Dlx6* locus as a site for dimethylation at H3-Lys9. We predict this sequence to be a key regulatory element for the *Dlx5-Dlx6* locus.

Higher-order organization of chromatin is important in gene expression³⁹. Chromatin looping as a result of remote sequences being brought close together might be involved in long-distance gene activation by locus control regions⁴⁰. In fact, chromatin looping was recently detected in the β -globin locus^{29,41}, the cytokine gene cluster⁴² and the *Igf2* locus⁴³. Our results show that distinct chromatin loop structures exist and can be correlated with the transcriptional status of chromatin, and that *Mecp2* is responsible for the formation of a silent chromatin-associated loop. *Mecp2* may have a function similar to that of *Satb1*, which is a cell type-specific gene regulator essential for T-cell development^{44,45}. *Satb1* has a role in tissue-specific organization of DNA sequences by folding chromatin by tethering specialized DNA sequences³⁹. Like *Mecp2*, *Satb1* targets Hdac1 as a component of chromatin-remodeling complexes to specific sites of genome and mediates region-specific histone mod-

ification^{39,46}. Mammalian MECP2 is homologous to chicken ARBP, which is a matrix attachment region (MAR)-binding protein that recognizes the central 5'-GGTGT-3' flanked by AT-rich sequences⁴⁷. The MAR-binding domain of ARBP is evolutionally conserved and includes the MBD of *Mecp2*. *Satb1* specifically recognizes base-unpairing regions conferred by an ATC sequence context that are often found in MARs⁴⁴. Therefore, both *Mecp2* and *Satb1* bind MARs despite the apparent difference in their sequence preference; this feature may be linked to some of the common functions of these two proteins.

In summary, our results show that *DLX* is a target gene of MECP2. *DLX5* is important in production of GABAergic neurons, suggesting that dysregulation of *DLX5* by mutation of *MECP2* might contribute to some of the phenotypes of RTT. Our data linking *Mecp2* to higher-order chromatin organization for silent chromatin provides a new mechanism for gene regulation by this repressor.

METHODS

Cloning of *in vivo* MBSs by urea-ChIP. We cloned *in vivo* MBSs from mouse brain using the procedure previously described for cloning of *in vivo* SATB1/*Satb1*-binding sequences²⁰ with some modifications. We crosslinked chromatin in 1-d-old brain cells, prepared by a 70- μ m cell strainer (BD Biosciences), by incubating cells in Dulbecco's modified Eagle medium containing 1% formaldehyde for 10 min at 37 °C followed by 1 h and 50 min at 4 °C. We purified crosslinked chromatin from free proteins and RNA by urea-gradient centrifugation. We digested the purified crosslinked chromatin with *Sau3AI* and precleared it by incubating the chromatin fragments with protein A-Sepharose 4B beads alone and then with nonimmune rabbit serum and protein A-Sepharose beads. We incubated the precleared chromatin with either nonimmune serum or antibody to *Mecp2* for 4 h at 4 °C and then with protein A-Sepharose 4B beads overnight at 4 °C and finally washed the chromatin fragments on beads four times with 1.0% Nonidet P-40 in phosphate-buffered saline and two times with washing buffer (10 mM Tris-HCl (pH 8.0), 250 mM LiCl, 0.5% Nonidet P-40, 0.5% sodium deoxycholate and 1 mM EDTA). We then digested the samples with 250 μ g ml⁻¹ proteinase K, treated them at 68 °C for 6 h to reverse crosslinking and subjected them to phenol-chloroform extraction before ethanol precipitation with glycogen. To determine whether any specific DNA sequences were bound to *Mecp2 in vivo*, we carried out PCR amplification using these two sets of DNA sequences (from DNA precipitated with antibody to *Mecp2* or with nonimmune serum) as templates. Primer sequences are available on request. To clone *in vivo* MBSs from brains, we carried out ligation-mediated PCR for the two sets of DNA at 20–25 cycles of PCR amplification so that PCR products could be obtained only from the DNA immunoprecipitated with antibody to *Mecp2*. We cloned the PCR products by TA cloning (Invitrogen) and determined the sequences. Our animal protocol was approved by the Animal Welfare and Regulatory Committee at Lawrence Berkeley Laboratory (AWRC number 12501).

Quantitative PCR analysis. We extracted total RNAs from the frontal cortex of *Mecp2*-null male mice (8 weeks old) using TRI REAGENT (Sigma) and treated them with RNase-free DNase I (Invitrogen). We carried out first-strand cDNA synthesis with an oligo(dT)₁₅ primer and Moloney murine leukemia virus reverse transcriptase (Promega). We carried out real-time RT-PCR on the LightCycler (Roche Diagnostics) with gene-specific primers and using SYBR Green I protocol. All reactions were done at least three times with the following cycling protocol: 10 min heat start at 95 °C and 40 cycles of denaturation at 95 °C for 10 s, annealing at 58 °C for 5 s and extension at 72 °C for 20 s. We carried out fluorescence detection at 72 °C. We normalized relative expression ratios to the housekeeping gene β -actin. Primer sequences are available on request.

Imprinting analysis. Primer sequences used for allele-specific expression analyses for *Calcr*, *Sgce*, *Peg10*, *Asb4* and *Dlx5* are available on request. We digested the total RNA samples with RNase-free DNase I to prevent DNA contamination. We incubated the total RNA with or without reverse

transcriptase, including an oligo (dT)₁₅ primer to confirm that no PCR amplification signals could be detected in the absence of reverse transcriptase. Genomic DNA and cDNA thus prepared were amplified by PCR with AmpliTaq Gold DNA polymerase (Applied Biosystems) using each of these primer sets and then by digested with *MnII* (for *Calcr*, *Peg10* and *Asb4*), *Tsp45I* (for *Sgce*) or *HindIII* (for *Dlx5*). These restriction sites were generated by SNPs and identified by sequencing PCR products derived from B6 and JF1 DNA templates. We analyzed the restriction fragments by PAGE and visualized them by staining with ethidium bromide for *Calcr*, *Sgce*, *Peg10* and *Asb4*. For *Dlx5*, we labeled PCR products by including 0.25 μl of [α -³²P]dCTP (10 mCi ml⁻¹) in each reaction. We resolved the *HindIII*-digested PCR products by 6% PAGE and quantified each band by Storm phosphorimager (Amersham Biosciences). We calculated the molar ratio of JF1 allele- and B6 allele-derived transcripts by normalizing the intensity of the two fragments to the number of cytosine residues in each of the PCR-amplified sequences.

Methylation analysis. We extracted genomic DNA by standard phenol-chloroform extraction methods and digested it with the appropriate restriction enzymes. We separated the resulting fragments on a 0.8% agarose gel and analyzed them by Southern-blot hybridization. We generated the probe by PCR from mouse genomic DNA. Primer sequences are available on request. We carried out bisulfite analysis as described³⁶. The CpG island of *DLX5* and the specific regions in mouse chromosome 6 that were chosen for the analysis are indicated in **Figure 4d** and **Supplementary Figure 2** online. We carried out the *HpaII*-*McrBC* PCR assay as described⁴⁸. We digested human genomic DNA (0.5 μg) with *HpaII*, *MspI* and *McrBC* (New England Biolabs) overnight at 37 °C. After purifying them, we subjected digested DNA fragments to PCR with AmpliTaq Gold DNA polymerase (Applied Biosystems). Primer sequences are available on request. All the reactions were done at least three times with the following cycling protocol: 10 min heat start at 95 °C and 32 cycles of denaturation at 95 °C for 30 s, annealing at 58 °C for 30 s and extension at 72 °C for 1 min. We separated the PCR products by electrophoresis on 1.5% agarose gel and stained them with ethidium bromide.

Cell culture for human lymphoblasts and allele-specific *DLX5* transcript analysis. We obtained LCLs from females with clinically diagnosed RTT from Coriell Cell Repositories. We selected LCLs from those individuals for whom LCLs from both parents were also available. We cultured individual cells in RPMI 1640 medium supplemented with 15% fetal bovine serum and 2 mM l-glutamine. We genotyped LCLs for the C7 or C8 mononucleotide repeat polymorphism located in the 3' UTR of *DLX5* to identify LCLs harboring the polymorphism, which permits the imprinting analyses of *DLX5*. Primer sequences are available on request. We obtained the PCR products using genomic DNA as templates and determined their DNA sequences. For *MECP2* expression analysis, we extracted total RNAs using TRI REAGENT and treated them with RNase-free DNase I. We carried out the first-strand cDNA synthesis with an oligo(dT)₁₅ primer as described in the previous section. We obtained the RT-PCR products and sequenced them directly using the original primers. We used the *IGF2* primer set and the *KCNQ1OT1* primer as described^{49,50}.

Expression of normal and mutant *MECP2* in LCLs. We determined the expression ratio of the wild-type and mutated *MECP2* alleles in each LCL sample by RT-PCR and direct sequencing of the genomic DNA containing the mutations. Primer sequences are available on request. For 1160(26del), we separated the RT-PCR products on a 6% polyacrylamide gel to analyze the mutated and wild-type *MECP2* transcripts.

Urea-ChIP assay for *in vivo* chromatin modification analysis. We used urea-ChIP throughout the chromatin-modification analysis across the 70-kb region containing the *Dlx5-Dlx6* locus. To determine histone modification patterns, we used antibodies to Mecp2, to acetylated H3-Lys9/Lys14, to dimethylated H3-Lys9 (Upstate Biotechnology) and to Hdac1 (BD Biosciences) for ChIP. We analyzed the urea-ChIP products for each region by real-time PCR using the LightCycler (Roche Diagnostics). We repeated all reactions at least three times with the following cycling protocol: 10 min heat start at 95 °C and 40 cycles of denaturation at 95 °C for 10 s, annealing at 58 °C for 5 s and extension at 72 °C for 20 s. Fluorescence detection was done at 72 °C. To quantify relative precipitated enrichments of the sequences in the 70-kb region in the chromatin

fragments immunoprecipitated with each specific antibody, we carried out real-time PCR for the ChIP DNA (immunoprecipitated chromatin pool) and whole-cell extracts (nonimmunoprecipitated chromatin). Primer sequences are available on request. We quantified the results by calculating the difference between the threshold cycle numbers for the ChIP DNA and for the whole-cell extracts as described³⁹.

ChIP-loop assay. We used crosslinked chromatin purified by urea ultracentrifugation (30 μg) as described above for this assay. We digested the purified crosslinked chromatin with a restriction enzyme (*PstI*) and precleared it as described above. We incubated precleared chromatin with nonimmune rabbit serum, antibody to Mecp2 (Upstate), antibody to dimethylated H3-Lys9 (Upstate) or antibody to acetylated H3-Lys9/Lys14 (Upstate) at 4 °C for 4 h and then incubated it with protein A-Sepharose 4B beads with rotation at 4 °C overnight. We washed complexes on beads four times with 1.0% Nonidet P-40 in phosphate-buffered saline and two times with washing buffer as indicated above. We resuspended the beads in 50 μl of ligation buffer and allowed DNA to be ligated overnight at 16 °C using T4 DNA ligase. We digested the samples sequentially with 100 $\mu\text{g ml}^{-1}$ RNaseA and 250 $\mu\text{g ml}^{-1}$ proteinase K, treated them at 68 °C for 6 h to reverse crosslinking and subjected them to phenol-chloroform extraction and then ethanol precipitation. We amplified ligated DNA with AmpliTaq Gold polymerase (Applied Biosystems) using 1 cycle of 94 °C for 9 min; and 30–35 cycles of 94 °C for 30 s, 60 °C for 40 s and 72 °C for 30 s; and 72 °C for 5 min. As internal controls for DNA amount, restriction enzyme digestion and proper subsequent ligation, we used two closely located neighboring fragments in the β -actin locus for transcriptionally active chromatin (acetylated H3-Lys9/Lys14) and the β -globin locus for silent chromatin (dimethylated H3-Lys9). We used two primers for the β -actin locus (primer sequences are available on request). The *PstI* sites between these two primers are separated by 1,623 bp. Upon *PstI* digestion and ligation, we expect to obtain a PCR product of 163 bp. We used two primers for the β -globin locus (primer sequences are available on request). The *PstI* sites between these two primers are separated by 720 bp and encompass an additional internal *PstI* site. Upon *PstI* digestion, we expect to obtain a PCR product of 154 bp. The PCR amplification occurs reproducibly, owing to the short distance. We confirmed all the ligation products by cloning the PCR products and then sequenced DNA of the insert. In addition to the ChIP-combined loop assay, we also carried out the 3C assay essentially as described²⁹, except that we used urea-purified crosslinked chromatin as the starting material. We confirmed that all PCR primer combinations could be properly amplified using the *PstI*-digested fragments of a BAC clone containing the 70-kb region, owing to the high molar concentration of fragments. Also, as a negative control, we determined that none of the primer combinations tested showed an amplified product using purified genomic DNA similarly digested with *PstI*. We ligated genomic DNA at 2.5 ng μl^{-1} in 500 μl of ligation buffer (similar to the conditions used for the 3C assay); for BAC DNA, this was done at 35 ng μl^{-1} .

Note: Supplementary information is available on the Nature Genetics website.

ACKNOWLEDGMENTS

We thank Y. Kohwi for valuable suggestions and F. Creegan, S. Krauss and the members of the laboratory for critical reading of the manuscript. This work was supported by an International Rett Syndrome Association Fellowship to S.H., a Rett Syndrome Research Foundation Fellowship to M.M. and by a US National Institutes of Health grant to T.K.-S.

COMPETING INTERESTS STATEMENT

The authors declare that they have no competing financial interests.

Received 23 August; accepted 22 November 2004

Published online at <http://www.nature.com/naturegenetics/>

- Li, E. Chromatin modification and epigenetic reprogramming in mammalian development. *Nat. Rev. Genet.* **3**, 662–673 (2002).
- Lewis, J.D. *et al.* Purification, sequence, and cellular localization of a novel chromosomal protein that binds to methylated DNA. *Cell* **69**, 905–914 (1992).
- Nan, X. *et al.* Transcriptional repression by the methyl-CpG-binding protein MeCP2 involves a histone deacetylase complex. *Nature* **393**, 386–389 (1998).

4. Jones, P.L. *et al.* Methylated DNA and MeCP2 recruit histone deacetylase to repress transcription. *Nat. Genet.* **19**, 187–191 (1998).
5. Fuks, F. *et al.* The methyl-CpG-binding protein MeCP2 links DNA methylation to histone methylation. *J. Biol. Chem.* **278**, 4035–4040 (2003).
6. Kimura, H. & Shiota, K. Methyl-CpG-binding protein, MeCP2, is a target molecule for maintenance DNA methyltransferase, Dnmt1. *J. Biol. Chem.* **278**, 4806–4812 (2003).
7. Amir, R.E. *et al.* Rett syndrome is caused by mutations in X-linked MECP2, encoding methyl-CpG-binding protein 2. *Nat. Genet.* **23**, 185–188 (1999).
8. Kriaucionis, S. & Bird, A. DNA methylation and Rett syndrome. *Hum. Mol. Genet.* **12**, R221–R227 (2003).
9. Shahbazian, M.D. & Zoghbi, H.Y. Rett syndrome and MeCP2: linking epigenetics and neuronal function. *Am. J. Hum. Genet.* **71**, 1259–1272 (2002).
10. Dragich, J., Houwink-Manville, I. & Schanen, C. Rett syndrome: a surprising result of mutation in MECP2. *Hum. Mol. Genet.* **9**, 2365–2375 (2000).
11. Shahbazian, M.D., Antalffy, B., Armstrong, D.L. & Zoghbi, H.Y. Insight into Rett syndrome: MeCP2 levels display tissue- and cell-specific differences and correlate with neuronal maturation. *Hum. Mol. Genet.* **11**, 115–124 (2002).
12. Chen, R.Z., Akbarian, S., Tudor, M. & Jaenisch, R. Deficiency of methyl-CpG binding protein-2 in CNS neurons results in a Rett-like phenotype in mice. *Nat. Genet.* **27**, 327–331 (2001).
13. Guy, J., Hendrich, B., Holmes, M., Martin, J.E. & Bird, A. A mouse *Mecp2*-null mutation causes neurological symptoms that mimic Rett syndrome. *Nat. Genet.* **27**, 322–326 (2001).
14. Shahbazian, M. *et al.* Mice with truncated MeCP2 recapitulate many Rett syndrome features and display hyperacetylation of histone H3. *Neuron* **35**, 243–254 (2002).
15. Tudor, M., Akbarian, S., Chen, R.Z. & Jaenisch, R. Transcriptional profiling of a mouse model for Rett syndrome reveals subtle transcriptional changes in the brain. *Proc. Natl. Acad. Sci. USA* **99**, 15536–15541 (2002).
16. Traynor, J., Agarwal, P., Lazzaroni, L. & Francke, U. Gene expression patterns vary in clonal cell cultures from Rett syndrome females with eight different MECP2 mutations. *BMC Med. Genet.* **3**, 12 (2002).
17. Lalonde, M. Parental imprinting and human disease. *Annu. Rev. Genet.* **30**, 173–195 (1996).
18. Drexell, R.A., Goddard, C.J., Thomas, J.O. & Surani, M.A. Methylation-dependent silencing at the H19 imprinting control region by MeCP2. *Nucleic Acids Res.* **30**, 1139–1144 (2002).
19. Balmer, D., Arredondo, J., Samaco, R.C. & LaSalle, J.M. MECP2 mutations in Rett syndrome adversely affect lymphocyte growth, but do not affect imprinted gene expression in blood or brain. *Hum. Genet.* **110**, 545–552 (2002).
20. Kohwi-Shigematsu, T., deBelle, I., Dickinson, L.A., Galande, S. & Kohwi, Y. Identification of base-unpairing region-binding proteins and characterization of their *in vivo* binding sequences. *Methods Cell Biol.* **53**, 323–354 (1998).
21. Ono, R. *et al.* Identification of a large novel imprinted gene cluster on mouse proximal chromosome 6. *Genome Res.* **13**, 1696–1705 (2003).
22. Okita, C. *et al.* A new imprinted cluster on the human chromosome 7q21-q31, identified by human-mouse monochromosomal hybrids. *Genomics* **81**, 556–559 (2003).
23. Hoshiya, H., Meguro, M., Kashiwagi, A., Okita, C. & Oshimura, M. *Calcr*, a brain-specific imprinted mouse calcitonin receptor gene in the imprinted cluster of the proximal region of chromosome 6. *J. Hum. Genet.* **48**, 208–211 (2003).
24. Piras, G. *et al.* *Zac1* (*Lot1*), a potential tumor suppressor gene, and the gene for epsilon-sarcoglycan are maternally imprinted genes: identification by a subtractive screen of novel uniparental fibroblast lines. *Mol. Cell Biol.* **20**, 3308–3315 (2000).
25. Mizuno, Y. *et al.* *Asb4*, *Ata3*, and *Dcn* are novel imprinted genes identified by high-throughput screening using RIKEN cDNA microarray. *Biochem. Biophys. Res. Commun.* **290**, 1499–1505 (2002).
26. Panganiban, G. & Rubenstein, J.L. Developmental functions of the *Distal-less/Dlx* homeobox genes. *Development* **129**, 4371–4378 (2002).
27. Jenuwein, T. & Allis, C.D. Translating the histone code. *Science* **293**, 1074–1080 (2001).
28. Dekker, J., Rippe, K., Dekker, M. & Kleckner, N. Capturing chromosome conformation. *Science* **295**, 1306–1311 (2002).
29. Tolhuis, B., Palstra, R.J., Splinter, E., Grosveld, F. & de Laat, W. Looping and interaction between hypersensitive sites in the active beta-globin locus. *Mol. Cell* **10**, 1453–1465 (2002).
30. Stuhmer, T., Anderson, S.A., Ekker, M. & Rubenstein, J.L. Ectopic expression of the *Dlx* genes induces glutamic acid decarboxylase and *Dlx* expression. *Development* **129**, 245–252 (2002).
31. Lalonde, M., Minassian, B.A., DeLorey, T.M. & Olsen, R.W. Parental imprinting and Angelman syndrome. *Adv. Neurol.* **79**, 421–429 (1999).
32. Chen, W.G. *et al.* Derepression of BDNF transcription involves calcium-dependent phosphorylation of MeCP2. *Science* **302**, 885–889 (2003).
33. Martinowich, K. *et al.* DNA methylation-related chromatin remodeling in activity-dependent BDNF gene regulation. *Science* **302**, 890–893 (2003).
34. International Molecular Genetic Study of Autism Consortium (IMGSAC). A genomewide screen for autism: strong evidence for linkage to chromosomes 2q, 7q, and 16p. *Am. J. Hum. Genet.* **69**, 570–581 (2001).
35. Budden, S.S. & Gunness, M.E. Bone histomorphometry in three females with Rett syndrome. *Brain Dev.* **23** Suppl 1, S133–S137 (2001).
36. Mager, J., Montgomery, N.D., de Villena, F.P. & Magnuson, T. Genome imprinting regulated by the mouse Polycomb group protein Eed. *Nat. Genet.* **33**, 502–507 (2003).
37. Kimura, M.I. *et al.* DLX5, the mouse homologue of the human-imprinted DLX5 gene, is biallelically expressed in the mouse brain. *J. Hum. Genet.* **49**, 273–277 (2004).
38. Lewis, A. *et al.* Imprinting on distal chromosome 7 in the placenta involves repressive histone methylation independent of DNA methylation. *Nat. Genet.* **36**, 1291–1295 (2004).
39. Cai, S., Han, H.J. & Kohwi-Shigematsu, T. Tissue-specific nuclear architecture and gene expression regulated by SATB1. *Nat. Genet.* **34**, 42–51 (2003).
40. Bulger, M. & Groudine, M. Looping versus linking: toward a model for long-distance gene activation. *Genes Dev.* **13**, 2465–2477 (1999).
41. Carter, D., Chakalova, L., Osborne, C.S., Dai, Y.F. & Fraser, P. Long-range chromatin regulatory interactions *in vivo*. *Nat. Genet.* **32**, 623–626 (2002).
42. Spilianakis, C.G. & Flavell, R.A. Long-range intrachromosomal interactions in the T helper type 2 cytokine locus. *Nat. Immunol.* **5**, 1017–1027 (2004).
43. Murrell, A., Heeson, S. & Reik, W. Interaction between differentially methylated regions partitions the imprinted genes *Igf2* and *H19* into parent-specific chromatin loops. *Nat. Genet.* **36**, 889–893 (2004).
44. Dickinson, L.A., Joh, T., Kohwi, Y. & Kohwi-Shigematsu, T. A tissue-specific MAR/SAR DNA-binding protein with unusual binding site recognition. *Cell* **70**, 631–645 (1992).
45. Alvarez, J.D. *et al.* The MAR-binding protein SATB1 orchestrates temporal and spatial expression of multiple genes during T-cell development. *Genes Dev.* **14**, 521–535 (2000).
46. Yasui, D., Miyano, M., Cai, S., Varga-Weisz, P. & Kohwi-Shigematsu, T. SATB1 targets chromatin remodelling to regulate genes over long distances. *Nature* **419**, 641–645 (2002).
47. Weitzel, J.M., Buhrmester, H. & Stratling, W.H. Chicken MAR-binding protein ARBP is homologous to rat methyl-CpG-binding protein MeCP2. *Mol. Cell Biol.* **17**, 5656–5666 (1997).
48. Yamada, Y. *et al.* A comprehensive analysis of allelic methylation status of CpG islands on human chromosome 21q. *Genome Res.* **14**, 247–266 (2004).
49. Mitsuya, K. *et al.* LIT1, an imprinted antisense RNA in the human *KVLQT1* locus identified by screening for differentially expressed transcripts using monochromosomal hybrids. *Hum. Mol. Genet.* **8**, 1209–1217 (1999).
50. Lee, M.P. *et al.* Loss of imprinting of a paternally expressed transcript, with antisense orientation to *KVLQT1*, occurs frequently in Beckwith-Wiedemann syndrome and is independent of insulin-like growth factor II imprinting. *Proc. Natl. Acad. Sci. USA* **96**, 5203–5208 (1999).